

Research on Effects of Geometry Parameters on Stability Zone of a Rotor Supported by Foil-Air Bearings Using an Improved Foil Model

Nguyen Minh Quan^{*}, Pham Minh Hai, Dinh Van Phong

Hanoi University of Science and Technology, No. 1, Dai Co Viet, Hai Ba Trung, Hanoi, Viet Nam

Received: August 27, 2018; Accepted: November 26, 2018

Abstract

Foil-air bearings have been drawing much scientists' attention to application into high-speed rotating machines for environmentally friendly performance. Due to their compliant foil structure, foil-air bearings are able to resist being seized-up (because of high heat or centrifugal effect), thereby lengthening their service time. However, during working time, foil-air bearings are supposed to demonstrate their non-linear effects that need investigating, especially on rotor's performance. In this paper, an improved foil dynamic model with bending moment included is proposed to determine the effective stiffness of foil structure. The results are compared to published experimental data. From that, influences of some geometry parameters on rotor's stability are investigated based on a model of turbocharger with foil-air bearings.

Keywords: foil-air bearing, effective stiffness, non-linear dynamics

1. Introduction

Foil-air bearings (FAB) have been widely studied and applied into turbomachinery thanks to their outstanding advantage [1,2]. For conventional air self-acting bearing, the radial clearance needs to be small enough for air pressure generation; however, seizing can occur because shaft growth (due to high temperature) can surpass this clearance. This kind of hard contact can be avoided by soft contact between shaft surface and a compliant foil structure in a foil air bearing as shown in Fig 1. When stationary, shaft can be forced to contact the foil by preload. As rotating, the foil is pushed away and shaft will be airborne by aerodynamic pressure. The compliant foil structure consists of two foil layers: a planar sheet metal (top foil) generates aerodynamic pressure and an outside foil (bump foil) acts as an elastic foundation (with the corrugated shape - bump foil - as the most commonly used). Both of these foils are open loops, which have one edge welded onto the bearing sleeve, and the other is free.

Before dynamic response of a FAB-rotor system is investigated theoretically through characteristic equations [2,3], the foil structure needs to be modelled to find out its stiffness. The bump stiffness was formulated in Roger Ku's [4] and Iordanoff's [5] research. However, the bending moment at contact points between bump ends and bearing sleeve was omitted while it needs to be considered in elastic deformation. In another way, Arghir [6] modelled the bump foil as a set of linear springs with different stiffnesses connecting together.

Nevertheless, the bump shape was presumed to remain circular even after load exertion. Furthermore, top foil and all the bumps are assumed to stay in contact all the time while there may be some zones where aerodynamic pressure can be lower than ambient pressure.

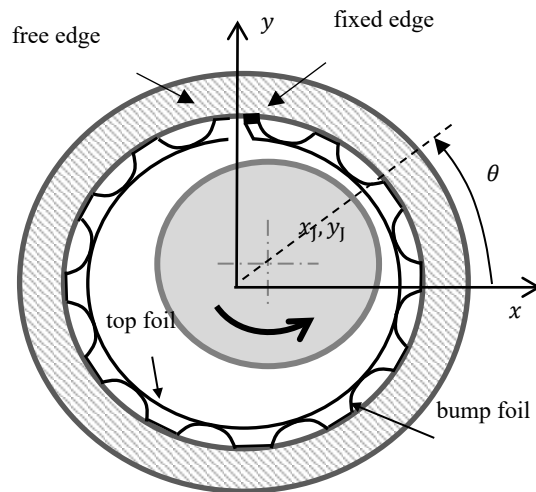


Fig. 1. Schematic diagram of a foil-air bearing

In this paper, bump stiffness is formulated taking bending moment at bump ends as well as change in curvature radius into account. From that, the effective stiffness of bearing is defined with real assumptions and compared with other experimental study. Then steady equilibrium state of a whole FAB-rotor system in a turbocharger is analyzed through evaluating effect of some geometry parameters.

^{*} Corresponding author: Tel.: (+84) 904.706.447
Email: quan.nguyenminh@hust.edu.vn

2. Governing equations

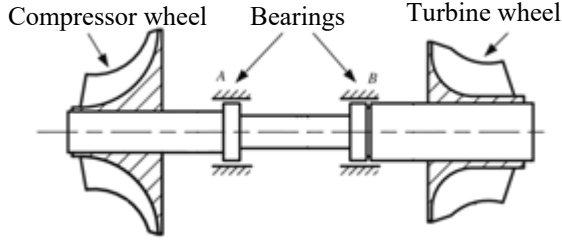


Fig. 2. Schematic diagram of a turbocharger shaft

A common turbocharger structure is illustrated in Fig 2, where the shaft is supported by two bearings. From the aspect of dynamic model, the rotor-FAB system can be analyzed into three subsystems which connect and interact with each other: rotor, air film and bump foil, as illustrated in Fig 3. The minor deflection of top foil can be neglected, and rotor is considered as a rigid body. As a result, three governing equations of motion can be established.

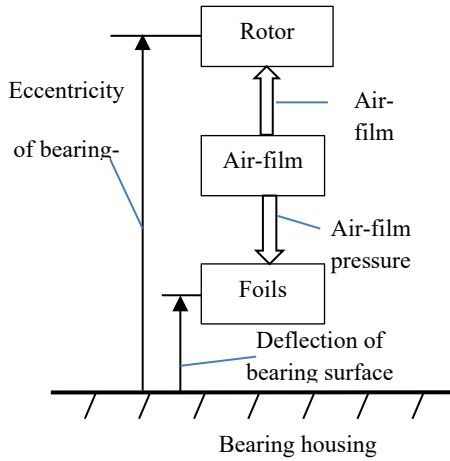


Fig. 3. Schematic diagram of a FAB-rotor system

The Reynold equation defining pressure distribution in the air film for compressible gas [7]:

$$\frac{\partial \psi}{\partial \tau} = \frac{1}{\Lambda} \left\{ \begin{array}{l} \frac{\partial}{\partial \theta} \left[\psi \left(\tilde{h} \frac{\partial \psi}{\partial \theta} - \psi \frac{\partial \tilde{h}}{\partial \theta} \right) \right] \\ + \frac{\partial}{\partial \zeta} \left[\psi \left(\tilde{h} \frac{\partial \psi}{\partial \zeta} - \psi \frac{\partial \tilde{h}}{\partial \zeta} \right) \right] - \frac{\partial \psi}{\partial \theta} \end{array} \right\} \quad (1)$$

where:

$$\psi = \tilde{p} \cdot \tilde{h}; \quad \tilde{h} = 1 - \varepsilon_x \cos \theta - \varepsilon_y \sin \theta + \tilde{w}$$

$$\tilde{w} = w/c; \quad \Lambda = \frac{6\mu\Omega}{p_a} \left(\frac{R}{c} \right)^2$$

The rotor displacement can be formulated as [8]:

$$\{\varepsilon''\} = \frac{1}{\Omega^2} (\{K_f\}\{f\} + \{S\} + [K_u]\{u\} + [K_g]\{\varepsilon'\}) \quad (2)$$

in which $\{\varepsilon\} = \{\varepsilon_{x1}, \varepsilon_{y1}, \varepsilon_{x2}, \varepsilon_{y2}\}^T$ denote the relative eccentricities of journal centers; $\{S\} = \{0, -g, 0, -g\}^T$ are gravitational force; $\{u\}$ are centrifugal forces; $\{f\} = \{F_{x1}, F_{y1}, F_{x2}, F_{y2}\}^T$ are reaction forces from air film.

The foil deflection is governed by the equation [9]:

$$\frac{d\tilde{w}(\theta)}{d\tau} = \frac{2}{\eta} \left(\frac{F(\theta)}{K_{td}} - \tilde{w}(\theta) \right) \quad (3)$$

where $K_{td} = k_b \cdot L \cdot c/p_a$ while k_b is the stiffness per unit area of the foil structure, L is bearing width, c is nominal clearance and p_a is ambient pressure; η is the loss factor and $F(\theta)$ is calculated by integrating pressure mesh along the axial direction.

It can be seen that stiffness of the foil plays an important role in determining foil deflection, while foil deflection \tilde{w} impacts the air film thickness, changing reaction forces and affecting rotor stability. Therefore, an improved foil structure model is used in this paper to determine the stiffness.

3. Analysis of improved foil structure model

3.1 Elasticity model of the bump foil

By the action of hydrodynamic pressure from air film, the foil structure is deformed. It was researched that the deformation of top foil (sagging effect [10]) was negligible and can be omitted. Therefore, only bump foil deformation is taken into account in this paper.

The difference in curvature under the action of bending moment can be described in the equation below [11]:

$$M = EI \cdot \left(\frac{1}{\rho_o} - \frac{1}{\rho} \right) \quad (4)$$

where ρ_o, ρ are the radii of curvature before and after bending, E is the elastic modulus of bump material, I is the moment inertia of cross section and M is the internal bending moment.

Under pressure from the top bearing foil, each bump of the supporting foil can respond in various modes. In this paper, three typical cases are considered, as shown in Fig. 4abc.

Discretizing the bump-foil model by n elements with length Δs along the length of the bump and using backward difference method result in the following equations, we have:

$$\frac{1}{\rho_i} = \frac{d\varphi}{ds} = \frac{\varphi_i - \varphi_{i-1}}{\Delta s} \quad (5)$$

Then, with X_N, Y_N - reaction forces at the end of the bump, equation (4) can be rewritten as follow.

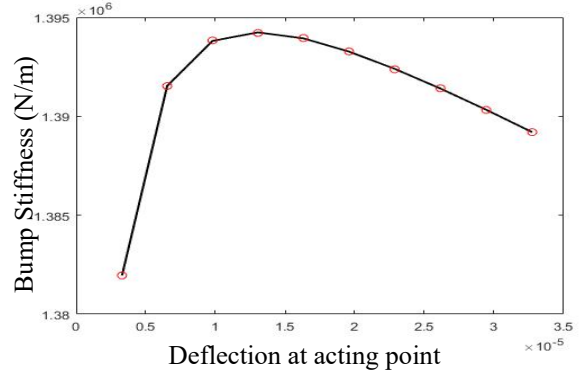
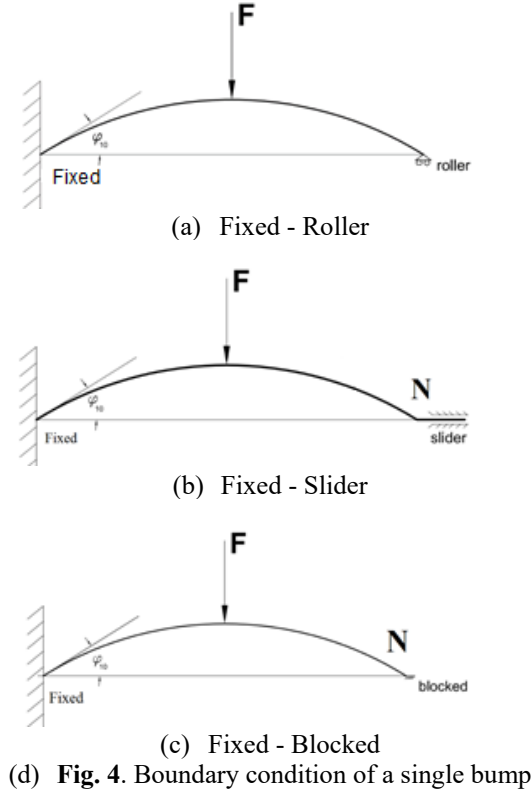


Fig. 5. Bump stiffness in case (a)

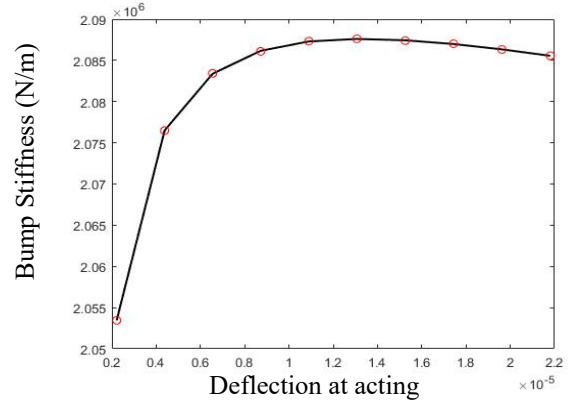


Fig. 6. Bump stiffness in case (b)

a) For elements from the right end to the acting point of the pressing force F

$$\frac{\varphi_i - \varphi_{i-1}}{\Delta s} = \frac{1}{EI} \left\{ X_N \sum_{i=1}^L a_i \cdot \sin \varphi_i \Delta s - Y_N \cdot \left(\sum_{i=1}^N b_i \cdot \cos \varphi_i \Delta s - \sum_{i=1}^L a_i \cdot \cos \varphi_i \Delta s \right) \right\} + \frac{1}{\rho_o} \quad (6a)$$

b) And for elements from the fixed end to the acting point of the pressing force F

$$\frac{\varphi_i - \varphi_{i-1}}{\Delta s} = \frac{1}{EI} \left\{ X_N \sum_{i=1}^L a_i \cdot \sin \varphi_i \Delta s - Y_N \cdot \left(\sum_{i=1}^N b_i \cdot \cos \varphi_i \Delta s - \sum_{i=1}^L a_i \cdot \cos \varphi_i \Delta s \right) - F \cdot \left(\sum_{i=1}^F c_i \cdot \cos \varphi_i \Delta s - \sum_{i=1}^L a_i \cdot \cos \varphi_i \Delta s \right) \right\} + \frac{1}{\rho_o} \quad (6b)$$

where N, F, L in sigmas define the elements at the end, at force F and at i^{th} element, respectively; with the boundary conditions are defined by:

- Case (a): $\begin{cases} y_N = 0 \\ \varphi_o = \varphi_{o1} \end{cases} \Leftrightarrow \begin{cases} \sum_{i=1}^L a_i \cdot \sin \varphi_i \Delta s = 0 \\ \varphi_o = \varphi_{o1} \end{cases}$
- Case (b): $\begin{cases} y_N = 0 \\ \varphi_o = \varphi_{o1} \end{cases} \Leftrightarrow \begin{cases} \sum_{i=1}^L a_i \cdot \sin \varphi_i \Delta s = 0 \\ \varphi_o = \varphi_{o1} \end{cases}$
- Case (c): $\begin{cases} y_N = 0 \\ \varphi_o = \varphi_{o1} \\ x_N = 0 \end{cases} \Leftrightarrow \begin{cases} \sum_{i=1}^L a_i \cdot \sin \varphi_i \Delta s = 0 \\ \varphi_o = \varphi_{o1} \\ \sum_{i=1}^L a_i \cdot \cos \varphi_i \Delta s = 0 \end{cases}$

Solving equations (5a,b) with one of the boundary conditions using Newton-Raphson algorithm for φ_i , the stiffness of the bump can then be calculated as follows:

$$K_{bump} = \frac{F}{v_F} \quad (7)$$

in which $v_F = y_{F0} - y_F$ is the deflection at the acting point of the force F .

Fig 5. shows the stiffness of one bump as a non-linear function of vertical displacement. As can be seen, there is a dramatic surge in the stiffness corresponding to early rise in displacement. This can be explained that the displacement is insufficient to overcome static state of the system, making the stiffness grow. In later periods, when the displacement continues increasing to prevail the static state, the bump end is gradually sloping, causing the stiffness to decrease (because the curvature radius increases).

The change tendency of the stiffness in case Fixed-Slider (Fig 6.) is deemed to be the same as in case Fixed-Roller. However, the decrease in later periods is slower because the curvature radius is forced to increase more quickly by roller than by slider

From Fig 7. there is no reduction in the stiffness when the displacement continues rising but it

significantly increases when the bump is blocked at the free end.

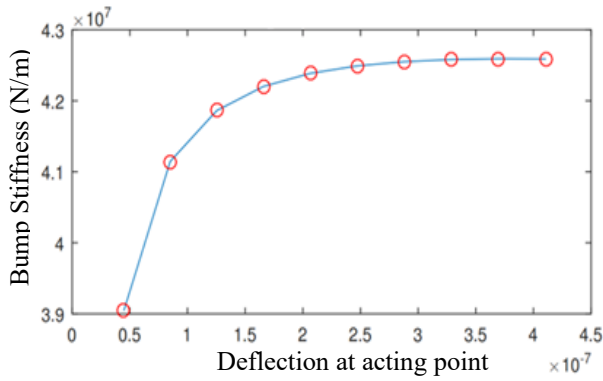


Fig. 7. Bump stiffness in case (c)

3.2 Effective stiffness of foil-structure

Since the bump foil is continuous, the effective stiffness of the bearing can be estimated using the roller-bearing approach. Fig. 8 shows the bump reaction forces onto the top foil when pressed down by the circular journal of the rotor.

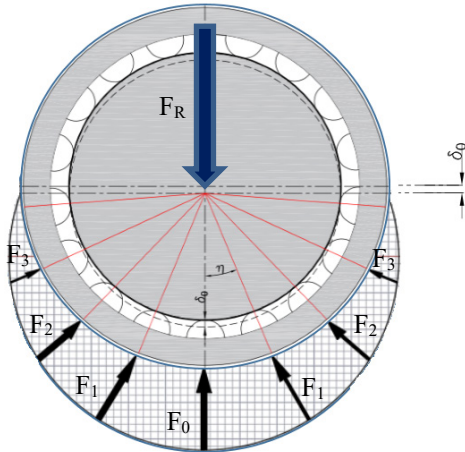


Fig. 8. Bump reaction forces

With a given deflection δ_0 of the center of shaft, the total force can be calculated by:

$$F_r = F_0 + 2F_1 \cos \eta + 2F_1 \cos(2\eta) + \dots + 2F_m \cos(m\eta) \quad (8)$$

where $F_i = K_{bump} \times \delta_i$

The effective stiffness of the bearing can be determined by:

$$K_{eff} = \frac{F_r}{\delta_0} \quad (9)$$

Some experimental coefficients and values shown in Table 1 are used for calculation of the effective stiffness in this paper. With the typical foil bearing presented in works done by Kim et al [3], the total effective stiffness of the foil structure is shown in Table 2.

Table 1. Main experimental parameters

Parameters	symbol	Value	Units
Air viscosity	μ	1.95×10^{-5}	N.s/m ²
Ambient pressure	p_a	101325	Pa
Nominal radial clearance	C_o	32	μm
Loss factor	η	0.25	
Number of bumps	n_{bump}	26	
Bump-foil thickness	t	102	μm
Rotor mass	m_r	3	kg

Table 2. Comparison of effective stiffness K_{eff}

Kim test data [2]	Fixed-roller (a)	Fixed-slider (b)	Fixed-blocked (c)
1.069E7	7.976E6	1.187E7	3.282E10

It has shown that the stiffnesses of elastic model in this paper with boundary conditions (a), (b) and from experiment by Kim [2] are nearly the same. The similarity has reinforced acceptable accuracy of the elastic model proposed by the authors. Remarkably, the stiffness shows a sharp increase in Case (c) where two ends of the bump are fixed and blocked.

4. Effect of geometry parameters

It is clearly that bump foil's geometry parameters have significant influence on the effective stiffness, leading to impact on rotor stability. For computation of K_{eff} , three important parameters of bump foil are considered: thickness (t), radius of the bump before bending (R_o) and number of bumps (n_{bump}).

Table 3. Computation of K_{eff} with different thickness

t (μm)	K_{eff} (N/m)
102	1.19×10^7
202	9.46×10^7
302	1.93×10^{11}
402	1.03×10^{14}
502	3.36×10^{15}
602	2.87×10^{16}
702	1.18×10^{17}
802	3.20×10^{17}
902	6.68×10^{17}
1002	1.19×10^{18}

From Table 3, it can be apparently observed that together with increasing thickness of the bump foil, the effective stiffness shows go-up tendency. Notably, corresponding to thickness of from 202 to 602 μm , there is a sharp rise in effective thickness, where the greatest increase is about 0.5×10^3 N/m.

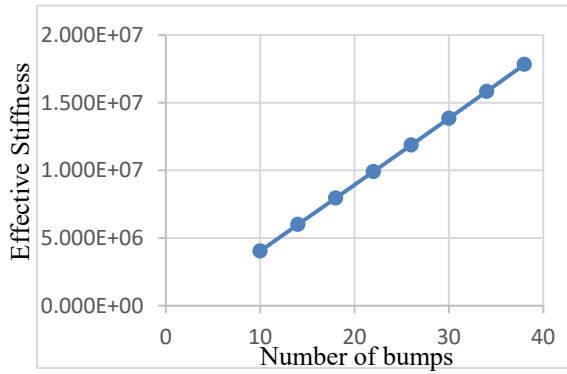


Fig. 9. Relationship between K_{eff} and number of bumps

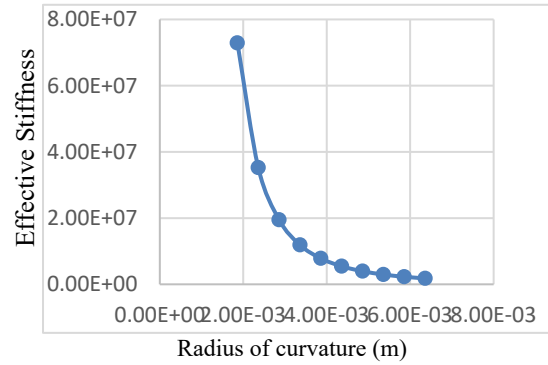


Fig. 10. Relationship of K_{eff} and radius of curvature

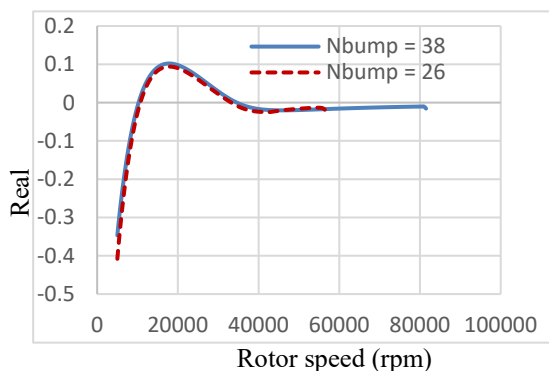
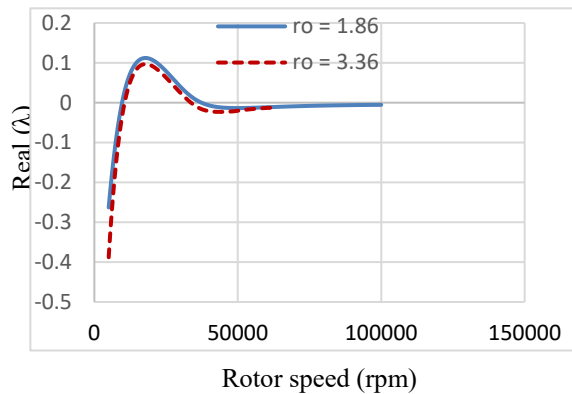
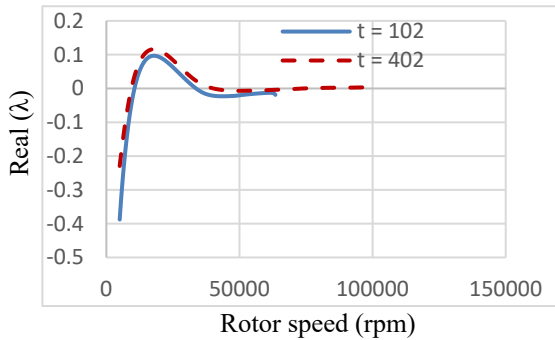


Fig. 11. Effect of geometry parameters on stability zone

Fig. 9. demonstrates a relatively linear relationship between effective stiffness and number of bumps. With bump quantity of from 10 to about 40, the effective stiffness of foil structure shows a gradual growth. It is argued that from assumption made in Fig.7, the number of bumps concerned in supporting the top foil increases, establishing more contact with the top foil, then causing smaller circumferential deflection.

Impact of radius of curvature on effective stiffness is illustrated in Fig 10. In general, the radius curvature does not have the same big influence on effective stiffness as the bump-foil thickness. From Fig. 9, it can be inferred that the more radius of curvature increases, the more effective stiffness decreases. This tendency can be reasoned that being acted by an up-to-down force, the outward movement of bump end is taken more easily with greater radius of curvature, causing bigger circumferential deflection.

Effect of geometry parameters on effective stiffness plays an important part in stability zone of rotor supported by foil air bearings.

In Fig. 11, λ is the leading eigenvalue of Jacobian of differential equations of motion (1,2,3) at an equilibrium. When $Re(\lambda) \leq 0$, rotor's motion is considered to be in equilibrium, while $Re(\lambda) > 0$, rotor will work unstably [10]. It can be seen that the general trend of rotor performance is in equilibrium at some starting revolutions, in unstable state when rotating faster, then back to equilibrium state again and maintain until certain revolutions. At low speed, thin gap between rotor and top foil forms an air film that is small enough to generate hydrodynamic pressure suffering rotor's weight, and the whole system performs in equilibrium state. At greater speed, first Hopf bifurcation occurs and the system moves to unstable state with orbit of limit cycle. When the speed gets higher, eccentricity of rotor center decreases due

to balance between air pressure and air-film thickness, the system perform in almost equilibrium state. However, when the speed reaches a certain value, the wedge shape of air film disappears and the equilibrium state is unable to maintain. In general, graphs in Fig.11 indicate that when the effective stiffness gets bigger, the system moves to unstable state more quickly, return to equilibrium state more slowly, but is able to maintain longer. With the thickness of 402 μm , the system returns to equilibrium state at around 40000 rpm and maintain up to 100000 rpm. Meanwhile, when the thickness of 102 μm , the system can only maintain up to about 63000 rpm. Similarly, in case the radius of curvature is 1.86 μm and number of bumps is 38, the system is able to remain in equilibrium state at 100000 rpm. The predicted performance can be reasoned that with higher stiffness, the deflection is smaller. Then, at starting speeds, the air-film thickness is smaller, generating higher hydrodynamic pressure, causing the system to move to unstable state faster. However, also with high stiffness, the eccentricity of rotor center decreases more slowly when returning to equilibrium state, helping the system to maintain at greater speed.

5. Conclusion

The paper has presented an improved model of foil structure and used some computing techniques to investigate effect of some geometry parameters on stability zone of rotor-FAB system. The results can be considered suggestions for designing and selecting suitable foil structure to apply foil air bearing into different situations.

6. Acknowledgement

This research is funded by the Hanoi University of Science and Technology (HUST) under project number T2017-PC-047.

References

- [1] G. L. Agrawal (1997) Foil Air/Gas Bearing Technology – An Overview, Proceedings of the ASME Turbo Expo, Orlando, Florida, USA, No. 97-GT-347
- [2] Daejong Kim (2007) Parametric Studies on Static and Dynamic Performance of Air Foil Bearings with Different Top Foil Geometries and Bump Stiffness Distributions, ASME Journal of Tribology, Vol. 129, April 2007
- [3] P. Bonello, H.M. Pham, (2014). The efficient computation of the nonlinear dynamic response of a foil-air bearing rotor system. *Journal of Sound and Vibration*, Vol 333(15) / 3459–3478.
- [4] Ku, C. P., Heshmat, H. (1992), Compliant Foil Bearings Structural Stiffness Analysis Part I: Theretical Model Including Strip and Variable Bump Foil Geometry, ASME Journal of Tribology, 114(2), pp. 394-400.
- [5] Iordanoff, I., (1999), Analysis of an Aerodynamic Compliant Foil Thrust Bearing: Method for a Rapid Design”, ASME Journal of Tribology, 121, pp. 816-822
- [6] S. Le Lez, M. Arghir, J. Frene (2007), A New Bump-Type Foil Bearing Structure Analytical Model, ASME Journal of Engineering for Gas Turbines and Power, Vol, 129, October 2007
- [7] Hai Pham, P. Bonello (2013) Efficient Techniques for thr Computation of the Nonlinear Dynamics of a Foil-Air Bearing Rotor System, Proceedings of ASME Turbo Expo 2013: Turbine Technical Conference and Exposition, Texas, USA
- [8] Pham Minh Hai, Nguyen Minh Quan, Nguyen Xuan Ha, Dang Bao Lam (2017), A parametric study on the effect of a discontinuous-foil air bearing on the dynamics of a turbomachine. Proceedings of the 11th SEATUC Symposium, Ho Chi Minh City, 2017.
- [9] Minh-Hai Pham, Xuan-Ha Nguyen, Bao-Lam Dang (2015), On the computation of the vibration of foil-air bearing – rotor systems. Proceedings of the 16th Asia Pacific Vibration Conference.
- [10] F. Xu, D. Kim, B. Z. Yazdi (2016), Theoretical Study of Top Foil Sagging Effect on the Performance of Air Thrust Foil Bearing, Proceedings of ASME Turbo Expo 2016: Turbomachinery Technical Conference and Exposition.
- [11] A. P. Chavan, Hong Zhou (2016), Analysis and Simulation of Slender Curved Beams, International Journal of Engineering Research & Technology, ISSN: 2278-0181, Vol. 5, pp. 214-221.